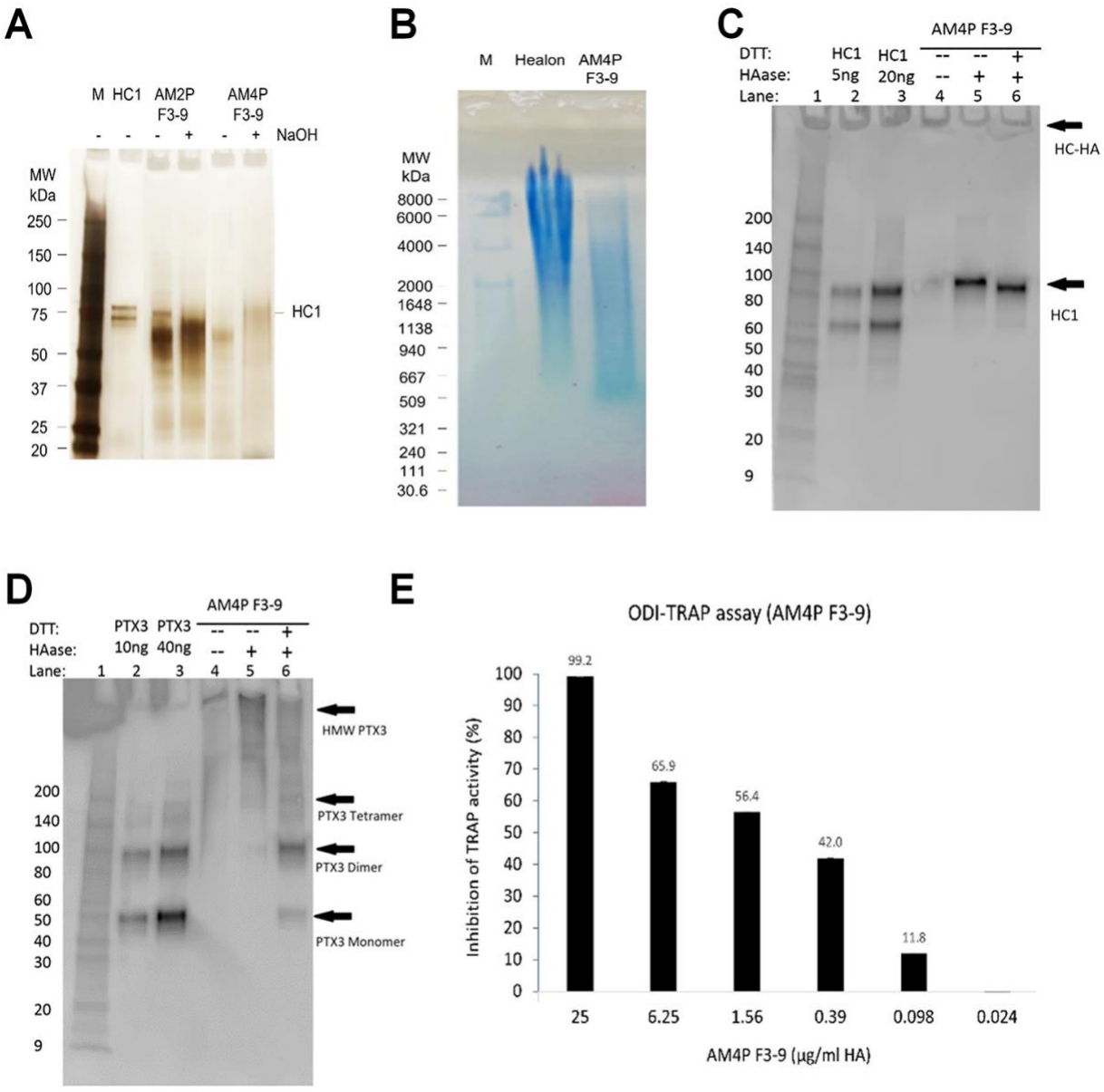

Fig. S1. Purification and characterization of HC-HA/PTX3.
(A) HC-HA/PTX3 was prepared from the human amniotic membrane by 2 runs (AM2P F3-9) or 4 runs (AM4P F3-9) of CsCl/4 M GnHCl ultracentrifugation and was then analyzed by silver staining. Each lane was loaded with 0.25 μg of HA without or with 100 mM NaOH treatment (25°C, 1 h) to cleave the bond between HA and HC1. (B) HC-HA/PTX3 (AM4P F3-9) purified from the amniotic membrane was electrophoresed on 0.5% agarose gel and stained with All-stains dye. Healon as a high-molecular-weight (HMW) HA control and HC-HA/PTX3 were loaded at 10 μg HA/lane; M: HA molecular weight ladder. (C-D) HC1 and PTX3 in HC-HA/PTX3 were detected by western blot using respective antibodies without (-) or with (+) hyaluronidase (HAase) treatment to release HC1 or HMW-PTX3, of which the latter can then be resolved into dimer or monomer without (-) or with (+) reduction with DTT. (E) Cloned murine RAW264.7

monocytes were seeded at 1x104 cells/cm2 in MEM α/10% FBS and differentiated into multi-nucleated osteoclasts with 25 ng/ml RANKL as the positive control and treated with HC-HA/PTX3 at different concentrations (0.024 – 25 μg/mL) for 3 days. The inhibition of TRAP activity in cell lysates was calculated as a percentage (%) of that of the positive control (shown on the top of each bar).

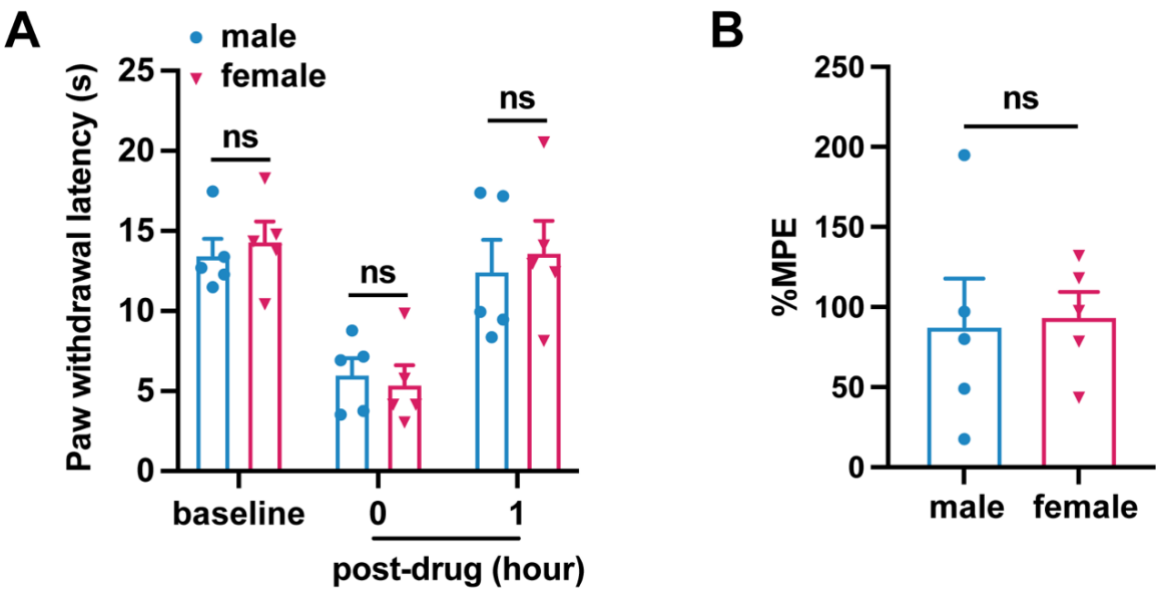

Fig. S2. HC-HA/PTX3 induced comparable inhibition of heat hyperalgesia in male and female mice after plantar incision.

(A) Paw withdrawal latency at different time point of male and female mice included in Figure 3B. (N= 5/sex) (B) The percentage of maximal possible effects (%MPE) at 1 hour post-drug were calculated for male and female mice included in Figure 3B. %MPE=1 - (baseline - post-drug) / (baseline - pre-drug). Data are mean ± SEM. (A) Two-way mixed model ANOVA followed by Bonferroni post hoc test. $^{*}P<0.05$ versus male. (B) Unpaired t-test.

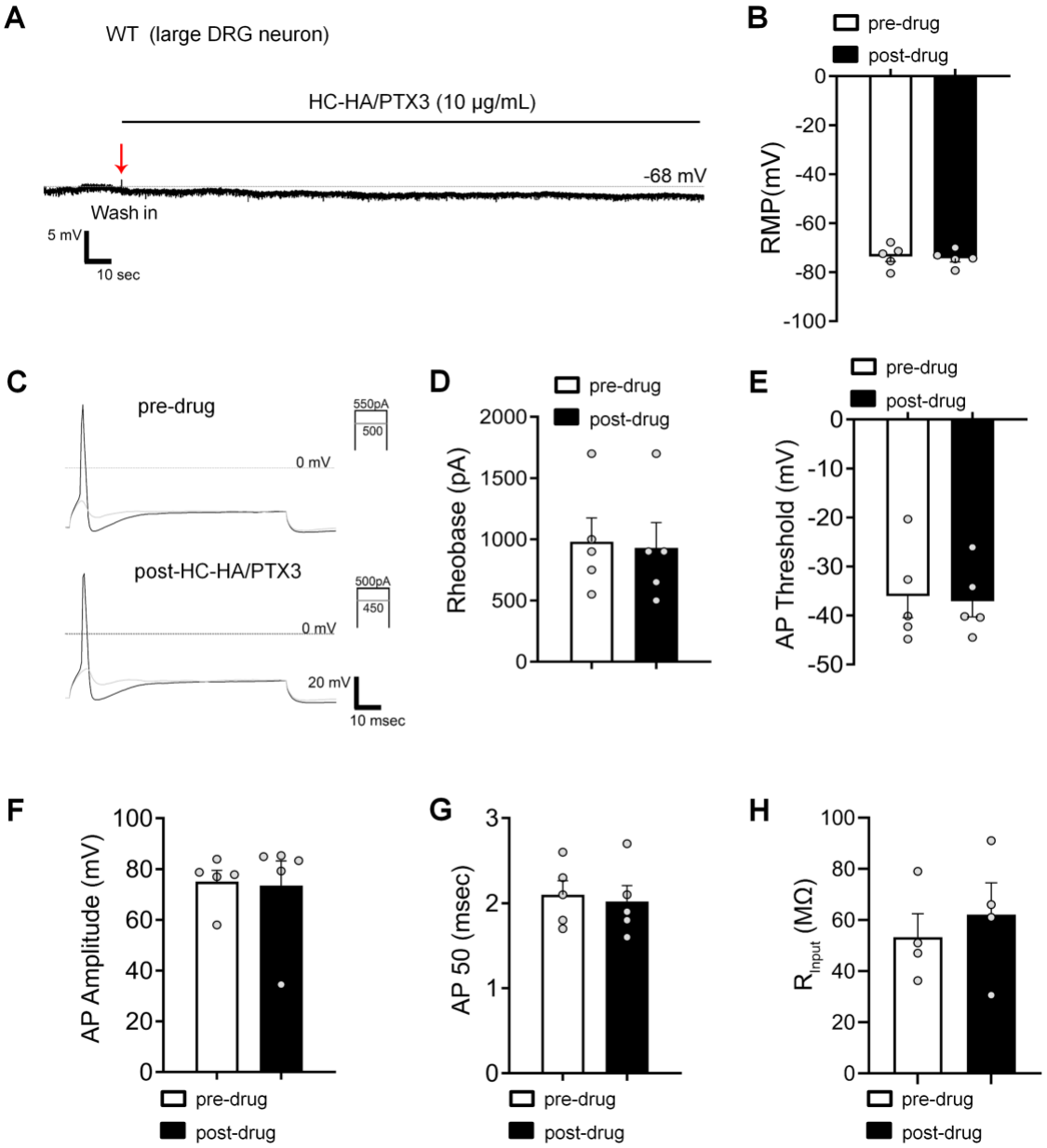

Fig. S3. HC-HA/PTX3 did not affect the excitability of large-diameter DRG neurons in wild-type (WT) mice after the plantar incision.

(A) The representative trace of membrane potential recorded under current-clamp conditions before and after HC-HA/PTX3 (15 µg/mL) treatment in a large DRG neuron of WT mice. Neurons were categorized according to cell body diameter as <20 µm (small), 20–30 µm (medium), and >30 µm (large). (B) The resting membrane potential (RMP) in large DRG neurons was not significantly changed at 5 min after HC-HA/PTX3 (10 µg/mL) treatment, compared to pre-drug (P=0.41). N=5. (C) Representative traces of rheobase measurements before and after HC-HA/PTX3 (10 µg/mL). (D-H) Quantification of the rheobase (D, P=0.09), action potential (AP) threshold (E, P=0.78), AP amplitude (F, P=0.8), AP duration (G, P=0.41), and the mean input resistance (Rinput, H, P=0.17) before and at 5 min after HC-HA/PTX3 (10 µg/mL) treatment. N=5. Data are

presented as mean ± SEM. (B, D-H) Paired t-test.

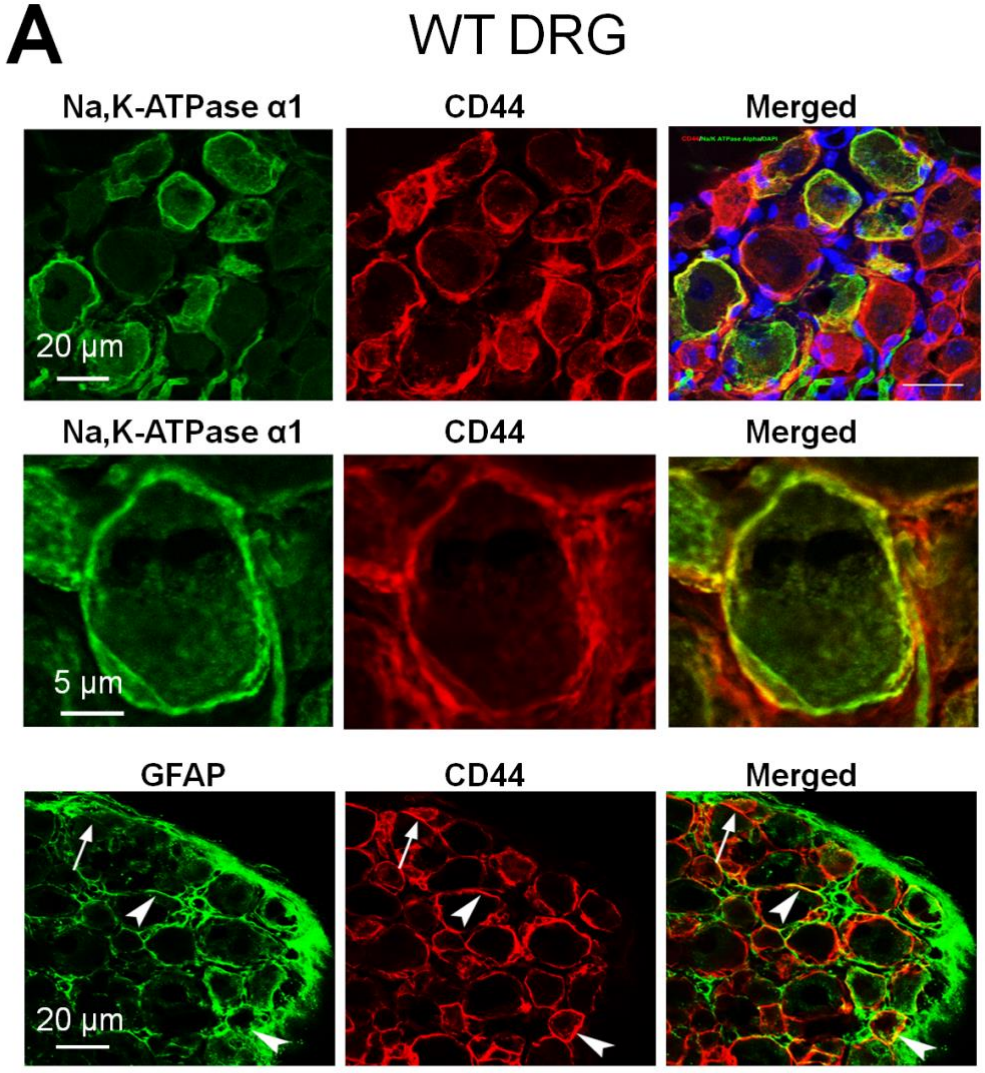

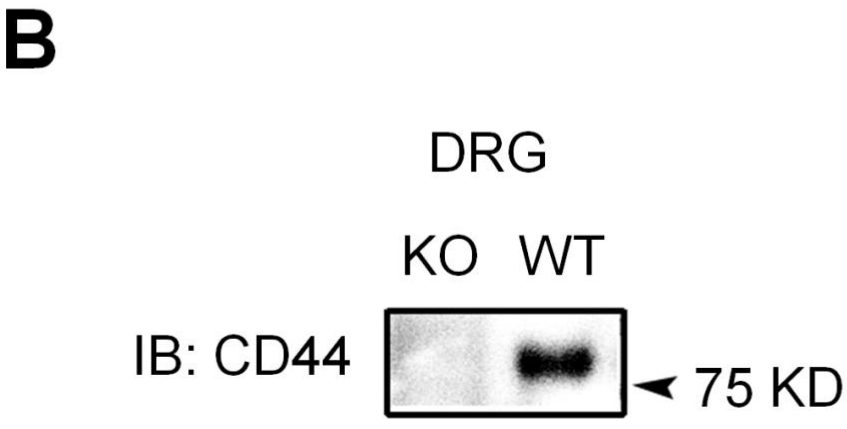

Fig. S4. The expression of CD44 in mouse DRG.
(A) Upper: Colocalization of CD44 and Na, K-ATPase alpha1 (a neuronal marker) immunoreactivity (IR) in wild-type (WT) mouse DRG. Blue: DAPI. Middle: A higher power view of CD44 and Na, K-ATPase alpha1 colocalization. Lower: Colocalization of CD44 and GFAP (a satellite glial cell marker) in DRG. Arrow: single-labeled cell; Arrowhead: double-labeled cell. (B) The specific CD44 band was not observed in the protein extracts derived from DRG tissues of CD44 knockout (KO) mice in the western blot study.

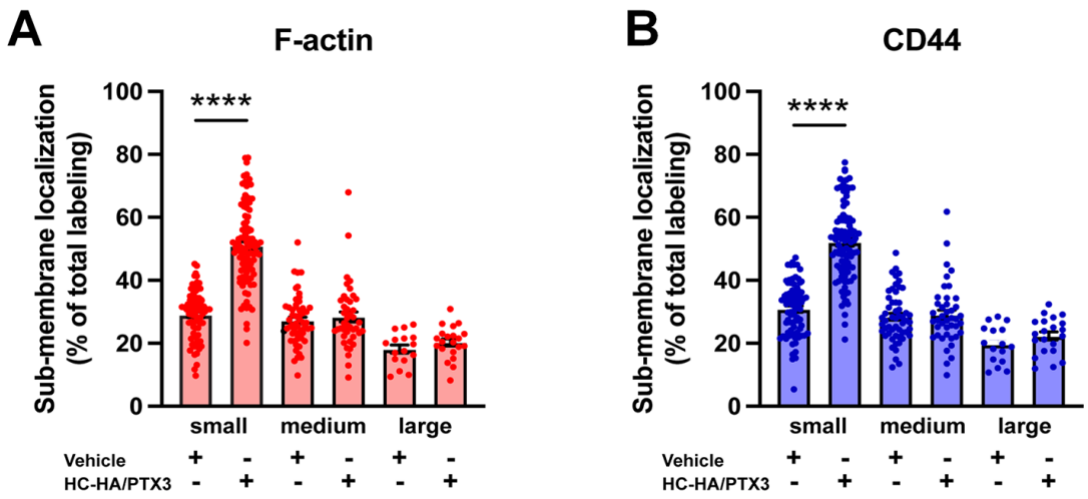

Fig. S5. Differential effects of HC-HA/PTX3 on sub-membranous F-actin polymerization and translocation of CD44 in small-, medium-, and large-diameter wild-type (WT) DRG neurons.

(A) Quantification of sub-membranous F-actin polymerization and (B) translocation of CD44 in different sizes of WT DRG neurons after HC-HA/PTX3 (10 μg/mL) or the vehicle (saline) treatment. DRG neurons were categorized according to cell body diameter as <20 μm (small), 20–30 μm (medium), and >30 μm (large). HC-HA/PTX3 increased sub-membranous F-actin polymerization and translocation of CD44 exclusively in small neurons. N=16-91/group. Data are mean ± SEM. One-way ANOVA followed by Bonferroni post hoc test. ****P< 0.0001 versus vehicle.

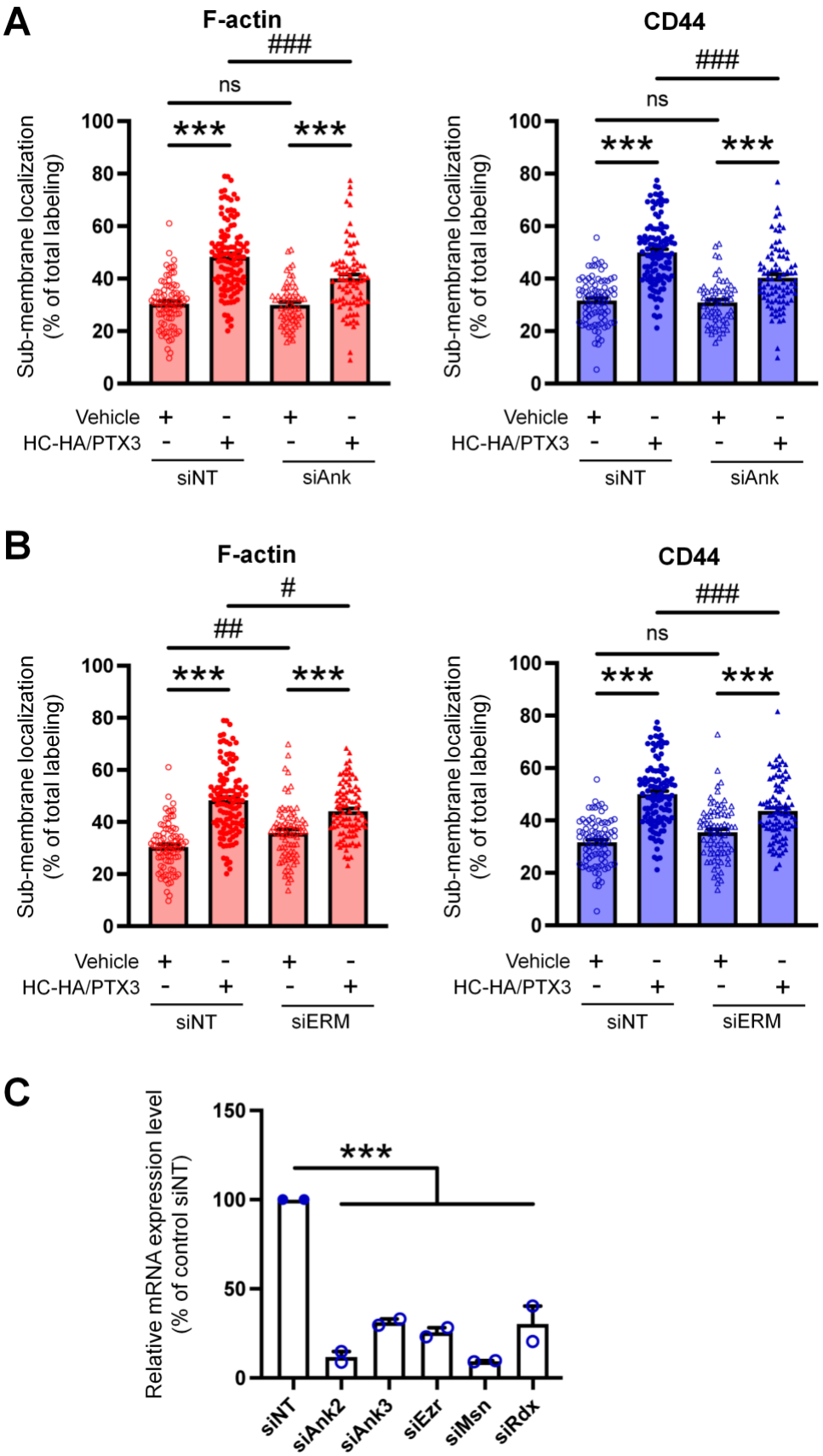

Fig. S6. Quantification of submembranous F-actin polymerization and translocation of CD44 in small-diameter wild-type (WT) DRG neurons in each group.
(A) DRG neurons were electroporated with siRNAs specifically targeting *Ank2* and *Ank3* (siAnk), (B) and those targeting *Ezr*, *Rdx*, and *Msn* (siERM) complex. Neurons were treated with a bath application of vehicle (saline) or HC-HA/PTX3 (10 μg/mL) for 45 min. N=59-114/group. (C) The mRNA expression of *Ank2*, *Ank3*, *Ezr*, *Msn*, and *Rdx* in DRG neurons electroporated with specific siRNAs were assayed by qPCR. N=2. Data are mean ± SEM. One-way ANOVA followed by Bonferroni post hoc test. ***P<0.001 versus vehicle; $^{###}$P<0.001 versus indicated group.

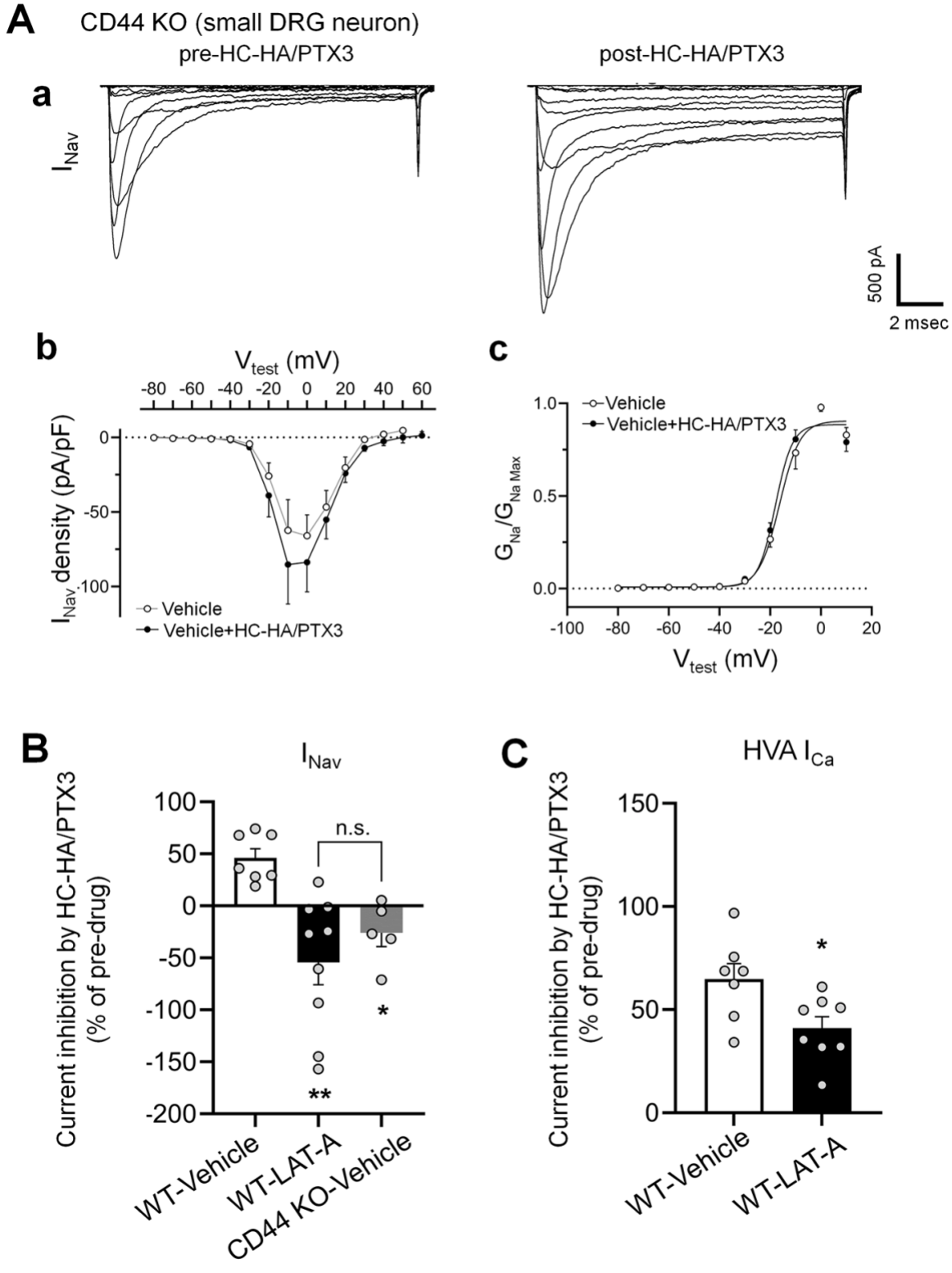

Fig. S7. The inhibitions of I_{Nav} by HC-HA/PTX3 in small-diameter DRG neurons were diminished in CD44 KO mice and were inhibited by a pre-treatment of LAT-A

in neurons from WT mice.

(A) HC-HA/PTX3 (10 µg/mL) did not inhibit I_{Nav} in small-diameter DRG neurons from CD44 KO mice. a. Representative traces of I_{Nav} in a CD44 KO neuron before and at 5 min after bath application of HC-HA/PTX3 (10 µg/mL). b. There was no significant change of I_{Nav} density (pA/pF) before and after HC-HA/PTX3 (10 µg/mL) treatment in CD44 KO neurons. c. HC-HA/PTX3 did not alter G_{Na}/G_{Na} max across the test voltages in CD44 KO neurons. N=5. (B) Changes of I_{Nav} after bath application of HC-HA/PTX3 (10 µg/mL) in vehicle-infused (N=7) and LAT-A-infused small WT DRG neurons ($P<0.01$, N=9), and in vehicle-infused CD44 KO neurons (N=5). DRG neurons were infused with the vehicle or LAT-A (0.5 nM) through the recording electrode, followed by bath application of HC-HA/PTX3 (10 µg/mL) 5 min later. The lumbar DRG neurons were harvested on Days 2-3 after the plantar incision. DRG neurons were categorized according to cell body diameter as <20 µm (small), 20–30 µm (medium), and >30 µm (large). Data are mean ± SEM. One-way ANOVA with Holm-Sidak post-test. $^{*}P < 0.05$, $^{**}P<0.01$ versus WT-vehicle pretreatment group. (C) The inhibition of HVA I_{Ca} by HC-HA/PTX3 (10 µg/mL) in vehicle-infused (N=7) and LAT-A-infused small WT DRG neurons ($P=0.02$, N=8). Data are mean ± SEM. Unpaired Student's t-test.

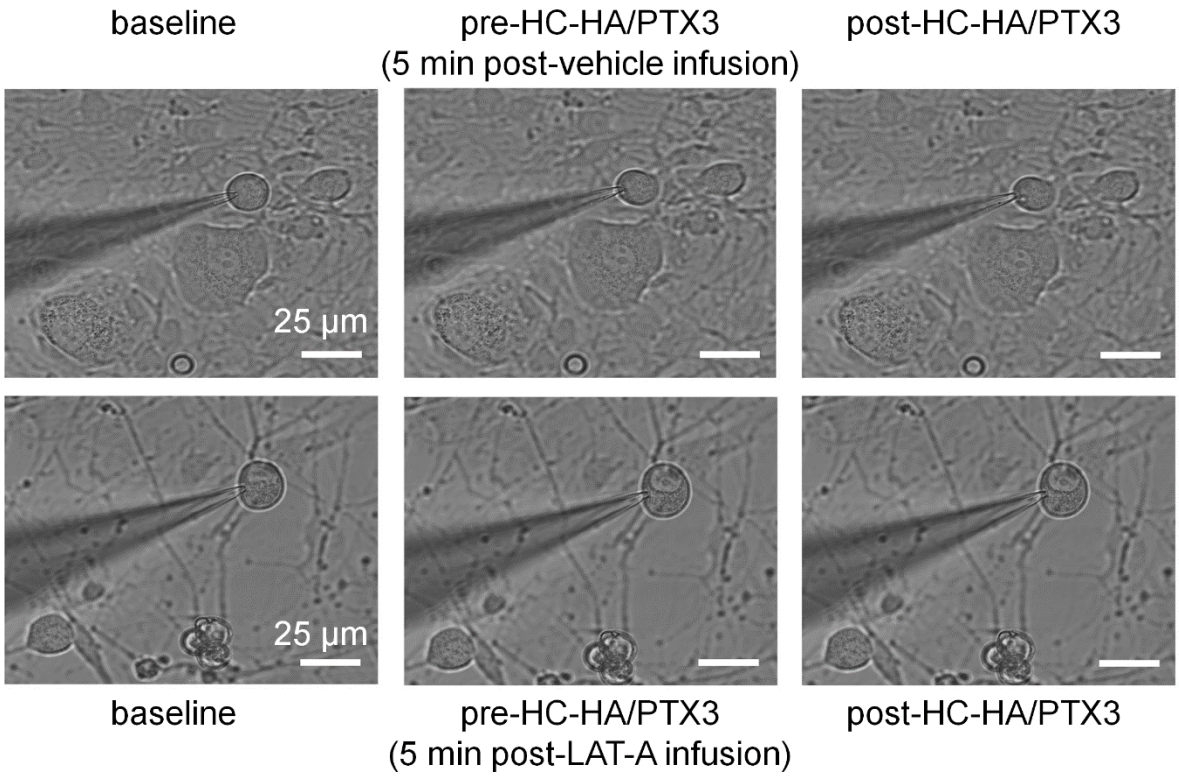

Fig. S8. Intracellular infusion of LAT-A did not change the gross morphology of DRG neurons in patch clamp recordings.
Example images show a small-diameter DRG neuron after infusion vehicle or Latrunculin A (LAT-A, 0.5 nM) through the recording electrode, followed by bath application of HC-HA/PTX3 (15 µg/mL). Scale bar: 25 µm. DRG neurons were categorized according to cell body diameter as <20 µm (small), 20–30 µm (medium), and >30 µm (large).

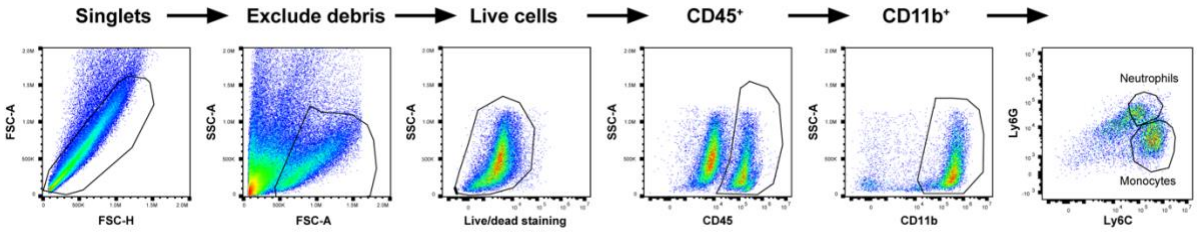

Fig. S9. Representative flow cytometry gating strategy for identification of $CD45^+$ cells, $CD11b^+Ly6G^+$ neutrophils, and $CD11b^+Ly6G^-Ly6C^+$ monocytes in wild-type mice hind paw skin after the plantar-incision.

Table S1. The measures of intrinsic membrane properties of small-diameter DRG neurons in WT and CD44 KO mice.

Knocking out of CD44 did not significantly alter the intrinsic membrane property of DRG neurons, as compared to that in WT mice.

	Wild Type	$CD44^{-/-}$		p-value
V_{rest} (mV)	-49.4 ± 1.4	-48.77 ± 2.1	$t_{(21)} = 0.76$	0.81
Rheobase (pA)	156.9 ± 14.1	154.2 ± 21.81	$t_{(22)} = 0.1$	0.92
AP Threshold (mV)	-32.76 ± 1.29	-31.4 ±1.22	$t_{(22)} = 0.58$	0.57
AP Amplitude (mV)	70.27 ± 4.53	54.55 ± 8.73	$t_{(22)} = 1.69$	0.1
AP50 (msecs)	8.85 ± 0.55	10.02 ± 1.27	$t_{(22)} = 0.98$	0.33
Overshoot (mV)	37.26 ± 4.66	52.8 ± 6.15	$t_{(24)} = 1.69$	0.1
AHP (mV)	-65.47 ± 1.03	-64.05 ± 1.13	$t_{(24)} = 0.71$	0.48
τ-AHP (msecs)	70.98 ± 7.93	56.18 ± 8.63	$t_{(24)} = 0.96$	0.35